Helmholtz-Zentrum Dresden-Rossendorf (HZDR)

HELMHOLTZ ZENTRUM
DRESDEN ROSSENDORF

Radial pressure forces in Euler-Euler simulations of turbulent bubbly pipe flows

Rzehak, R.; Liao, Y.; Meller, R.; Schlegel, F.; Lehnigk, R.; Lucas, D.;

Originally published:

April 2021

Nuclear Engineering and Design 374(2021), 111079

DOI: https://doi.org/10.1016/j.nucengdes.2021.111079

Perma-Link to Publication Repository of HZDR:

https://www.hzdr.de/publications/Publ-32095

Release of the secondary publication
on the basis of the German Copyright Law § 38 Section 4.

CC BY-NC-ND

Radial pressure forces in Euler-Euler simulations of turbulent bubbly pipe flows

Roland Rzehak*, Yixiang Liao, Richard Meller, Fabian Schlegel, Ronald Lehnigk, Dirk Lucas

Helmholtz-Zentrum Dresden – Rossendorf, Institute of Fluid Dynamics,
Bautzner Landstrasse 400, D-01328 Dresden, Germany

Abstract

Two-equation turbulence models based on the Boussinesq eddy viscosity hypothesis that have been used in the vast majority of previous simulation studies on bubbly pipe flows contain a term which renders the radial pressure distribution non-constant. In single phase simulations this effect is invariably absorbed in the definition of a modified pressure, from which the real pressure may be recovered if necessary. For bubbly multiphase flows however, this is not possible since the bubbles experience a force which depends, of course, on the real pressure rather than the modified one. As it turns out, most software codes by default rely on the approximation of neglecting the difference between modified and real pressure for bubbly flows. The purpose of the present study is to assess the influence of this approximation on the final simulations results. Fortunately it turns out that at least for the conditions considered in this study, the error is small.

Keywords: turbulent dispersed gas liquid multiphase flow, Euler-Euler two fluid model, closure relations, CFD simulation, model validation, bubbly pipe flow

* Corresponding author. E-mail: r.rzehak@hzdr.de

TABLE OF CONTENTS

1 INTRODUCTION

Bubbly flows are common in many engineering disciplines comprising chemical engineering, biotechnology and energy production. In such systems, the exchange of momentum, heat, and mass between the phases poses a complex multiphysics problem. Consequently, design and optimization of technical equipment involving bubbly flow present a great challenge. In this situation, CFD simulations bear the potential of identifying energy- and resource- efficient solutions which are prohibitively expensive and time-consuming to be uncovered by conventional semi-empirical methods.

CFD simulations of dispersed bubbly flow on the scale of technical equipment are feasible within the Eulerian two-fluid framework of interpenetrating continua. Since phenomena occurring on the scale of individual bubbles or groups thereof are not resolved in this approach, accurate numerical predictions rely on suitable closure relations describing the physics of these small-scale phenomena. As a first step towards a predictive model, a set of baseline closures applicable to adiabatic bubbly flows has been proposed in Rzehak and Krepper (2013) comprising the exchange of momentum between liquid and gas phases and the effects of the dispersed bubbles on the turbulence of the liquid carrier phase. This baseline model has subsequently been validated for a large number of test cases (e.g. Lucas et al. 2016, Liao et al. 2018, and references therein). Improving its accuracy (Ma et al. 2017, Krepper et al. 2018, Liao et al. 2019) and extending its range of applicability (e.g. Liao et al. 2015, Rzehak and Krepper 2016, Krauß and Rzehak 2018, Shi and Rzehak 2018, Fleck and Rzehak 2019) are ongoing efforts.

In a very recent work, likewise concerned with closure relations for the two-fluid description of bubbly flows, Colombo and Fairweather (2019) emphasized the role of the Reynolds-stress gradient in determining the lateral distribution of the gas fraction in various pipe flows, in particular the well-known wall-peaking. It has been known for a long time that a non-constant pressure distribution results from the Reynolds-stress gradient (Wang et al. 1987). This in turn results in a pressure gradient force pushing the gas bubbles towards a wall in pipe flows. An advanced elliptic-blending Reynolds-stress model was used by Colombo and Fairweather (2019) to capture this effect and taking only turbulent dispersion into account to provide a counteracting tendency, they obtained a remarkable similarity of simulated and measured gas fraction profiles for a number of test cases. To aid further understanding, an equation for the gas fraction profile was derived for fully developed axisymmetric flow following Ullrich et al. (2014). Two terms appear in this equation, an isotropic and an anisotropic one. Of these, the former is also present in simpler two-equation turbulence models as used in the above-mentioned baseline closure. Upon closer inspection it was found however, that this term is frequently neglected due to the default settings in major software codes. The purpose of the present study is to assess the consequences of such an approximation.

The paper is organized as follows. A precise statement of the problem together with a summary of the necessary theoretical background is given in section 2. The applied baseline closure model is summarized in section 3 with references to more detailed presentations that have been given previously. For the assessment several previously investigated test cases have been selected. These are described together with the simulation setups and the results in section 4. Conclusions are offered in section 5.

2 THEORETICAL BACKGROUND AND PROBLEM DESCRIPTION

Focusing first on single-phase flows, two-equation turbulence models like the k-ε (Launder and Spalding, 1974), k-ω (Wilcox, 1988), or SST model (Menter 2009) are based on the Boussinesq eddy viscosity hypothesis expressing the turbulent Reynolds stress for an incompressible flow as (Wilcox, 2006, ch 4.1)

$$\mathbf{T}^{turb} = \mu^{turb}(\nabla \boldsymbol{u} + (\nabla \boldsymbol{u})^T) - \frac{2}{3}\rho k\, \mathbf{1}, \qquad (1)$$

where $\mathbf{1}$ denotes the identity tensor. Here, the first term embodies the idea that turbulence acts in a diffusive way similar to molecular fluctuations. The second term is needed to get the correct trace, since the contribution from the first term vanishes for incompressible flow with $\nabla \cdot \boldsymbol{u} = 0$, but from the definition $\mathbf{T}^{turb} = -\rho \boldsymbol{u}' \otimes \boldsymbol{u}'$ together with $k = |\boldsymbol{u}'|^2/2$ one should have $tr(\mathbf{T}^{turb}) = -2\rho k$. Together with the viscous contribution

$$\mathbf{T}^{vis} = -p\mathbf{1} + \mu^{mol}(\nabla \boldsymbol{u} + (\nabla \boldsymbol{u})^T), \qquad (2)$$

the total stress then becomes

$$\mathbf{T} = \mathbf{T}^{vis} + \mathbf{T}^{turb} = -p^{mod}\mathbf{1} + \mu^{eff}(\nabla \boldsymbol{u} + (\nabla \boldsymbol{u})^T), \qquad (3)$$

where $p^{mod} = p + \frac{2}{3}\rho k$ and $\mu^{eff} = \mu^{mol} + \mu^{turb}$. The advantage of this formulation is that CFD codes for laminar flow may be used to compute the mean flow under turbulent conditions simply by replacing real pressure p with modified pressure p^{mod} and molecular viscosity μ^{mol} by effective viscosity μ^{eff}. The last term in Eq. (1) is hidden in the computation of the modified pressure as part of the numerical solution.

At solid walls the modified pressure equals the real pressure as turbulent kinetic energy vanishes in this region. Therefore body forces can be correctly calculated by integration over the surface of a solid object. Should the real pressure be needed inside the computational domain it can easily be obtained from the computed solution variables as a post-processing step. As sketched in Figure 1, in pipe flows the modified pressure is uniform over the cross-section and the turbulent kinetic energy increases from the pipe center towards the wall until the viscous sublayer is reached (Pope, 2000 ch 7.1). Thus the real pressure decreases from the pipe center towards the wall outside the viscous sublayer.

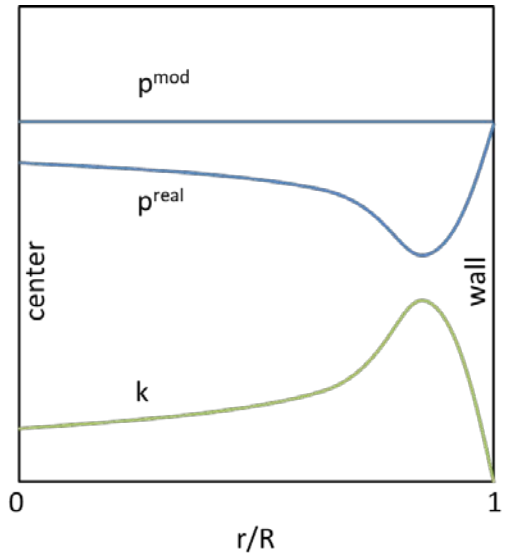

Figure 1: Qualitative sketch of the radial dependence of real and modified pressures in pipe flow.

For multiphase flows, a bubble experiences among others a force proportional to the negative gradient of real pressure in the surrounding fluid (Maxey and Riley, 1983). Hence, in a turbulent pipe flow, a force pushing the bubble towards the pipe wall arises from the radial variation of turbulent kinetic energy. In the two-fluid model, a term corresponding to this pressure gradient force acting on the bubbles appears in the gas phase momentum equation. However since there is only a single pressure for both phases (see next section) this term cannot be evaluated after the solution has been computed. For this reason, the turbulent contribution to the pressure gradient force, i.e. the last term in Eq. (1), cannot be hidden in the computation of a modified pressure. Either it appears explicitly in the equations or its effect on the bubble motion will be neglected.

Looking first at ANSYS CFX as an example of a commercial CFD code frequently employed for bubbly flow computations it is found that the default setting is to neglect the turbulent contribution to the pressure gradient force, but including it can be enforced by setting an appropriate "expert parameter" (ANSYS, 2018). Likewise, examining the Euler-Euler solvers of OpenFOAM (OpenFOAM, 2018) as an example of an open source code with increasing use in the area, it is found that the turbulent contribution to the pressure gradient force is dropped in the code. Thus, many previous calculations have been performed without taking this effect into account and the question arises to which degree the obtained results are influenced by this approximation. In order to investigate this issue, the changes necessary to use the real pressure have been implemented in reactingMultiphaseEulerFoam solver of OpenFOAM.

To be precise, a term $-\frac{2}{3}\nabla\left(\alpha_\phi \rho_\phi k_\phi\right)$ is added generically to the right hand side of all phasic momentum equations (see below). However, as described in section 3 in the presently used baseline model, turbulence is considered only in the liquid phase so that $k_\phi \equiv 0$ except for $\phi = L$. In order to prevent excessive numerical error and oscillatory behavior, the discretization of this term has to match the discretization of the pressure term exactly, i.e. the same discrete approximation to the gradient operator has to be used. Care also needs to be taken with the typical outflow boundary condition assuming fully developed flow. In this case as noted above, the real pressure varies along the outlet boundary. Thus to ensure a smooth outflow at the outlet boundary, a fixed value needs to be specified for the modified pressure instead. Then, values for the real pressure are calculated as

$$p = p^{mod} - \frac{2}{3}\alpha_L \rho_L k_L, \tag{4}$$

and these are imposed as pressure boundary condition.

3 MODEL DESCRIPTION AND NUMERICAL SETUP

The physical models used for the simulations are exactly the same as used in a number of previous studies. Since extensive descriptions have been presented repeatedly, only a rather concise summary is given here for the sake of completeness together with references to the original works. Material properties, geometry, and boundary conditions suitable for the present application are specified.

The conservation equations for two-phase flow are summarized as follows (e.g. Drew and Passman 1998, Yeoh and Tu 2010, Ishii and Hibiki 2011).

The phasic continuity equations read

$$\frac{\partial}{\partial t}\left(\alpha_\phi \rho_\phi\right) + \nabla \cdot \left(\alpha_\phi \rho_\phi \boldsymbol{u}_\phi\right) = 0 \tag{5}$$

while the phasic momentum equations are

$$\begin{aligned}\frac{\partial}{\partial t}\left(\alpha_\phi \rho_\phi \boldsymbol{u}_\phi\right) + \nabla \cdot \left(\alpha_\phi \rho_\phi \boldsymbol{u}_\phi \otimes \boldsymbol{u}_\phi\right) \\ = -\alpha_\phi \nabla p + \nabla \cdot \left(\alpha_\phi \mathbf{S}_\phi\right) + \alpha_\phi \rho_\phi \boldsymbol{g} + \boldsymbol{F}_\phi^{inter}\end{aligned} \tag{6}$$

Here, $\phi = G, L$ denotes the respective phase, gas or liquid. Note that only a single pressure appears for all phases and of course the phase fractions are related as $\alpha_G + \alpha_L = 1$.

The term $\boldsymbol{F}_\phi^{inter}$ in Eq. (6) account for the momentum transfer between the phases. Due to momentum conservation the relation $\boldsymbol{F}_G^{inter} = -\boldsymbol{F}_L^{inter}$ holds. According to the baseline model applied herein, it comprises of a number of contributions summarized in Table 1 together with the closure correlation used for each. Further details and validation studies can be found e.g. in Ziegenhein et al. (2013), Rzehak et al. (2015), Liao et al. 2016, Rzehak and Krepper (2015), Rzehak et al. (2017a), or Liao et al. (2018).

Table 1: Summary of bubble force correlations.

force	reference
drag	Ishii and Zuber (1979), single bubbles
shear lift	Tomiyama et al. (2002)
wall lift	Hosokawa et al. (2002)
turbulent dispersion	Burns et al. (2004)
virtual mass	constant coefficient C_{VM} = ½

The deviatoric stress tensor $\mathbf{S}_\phi$ according to the Boussinesq hypothesis is given by

$$\mathbf{S}_\phi = \left(\mu_\phi^{mol} + \mu_\phi^{turb}\right)\left(\nabla \boldsymbol{u}_\phi + \left(\nabla \boldsymbol{u}_\phi\right)^T\right) - \frac{2}{3}\rho_\phi k_\phi \mathbf{1}. \tag{7}$$

For the liquid phase, $\phi = L$, two models will be compared. In the first one, the last term in Eq. (7) is included such that p in Eq. (6) represents the real pressure. In the second one, this term is neglected and hence, p in Eq. (6) represents the modified pressure. In the following these two models will be referred to as “real pressure” and “modified pressure” models, respectively. As mentioned above, the latter is the default in many CFD software packages. In both cases, the turbulent dynamic viscosity for the liquid phase μ_L^{turb} is calculated from a SST model with additional source terms accounting for the bubble- induced turbulence according to Ma et al. (2017). Due to the low density and small spatial scales of the bubbles,

turbulence may be neglected for the gas phase. Thus for the gas phase, $\phi = G$, the last term in Eq. (7) is omitted and μ_G^{turb} is set to zero. Further details on the turbulence modeling are given e.g. in Rzehak and Krepper (2013a), Ziegenhein et al. (2017), Parekh and Rzehak (2018) or Liao et al. (2019).

All investigated tests are concerned with vertical upward flow of air bubbles in water in round pipes. A sketch of this general configuration is shown in Figure 2, where D gives the pipe diameter and H the length of the test section.

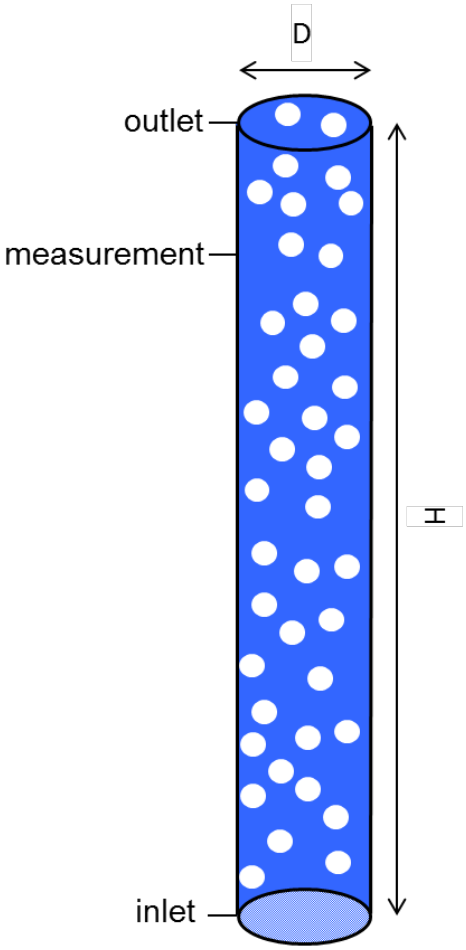

Figure 2: Sketch of the bubbly pipe flow geometry.

Simulations are performed in a quasi-2D geometry considering only a narrow cylindrical sector with symmetry boundary conditions imposed on the side faces. This simplification is frequently used for axisymmetric flows, for which it provides a good approximation. At the bottom of the domain, the profile for the liquid flow is set according to a typical single phase turbulent flow profile in a pipe as an inlet condition. Gas volume fraction and mass flux are set to uniform values at the inlet. Precise conditions at the inlet do not matter as long as the axial distance to the measurement location is large enough for fully developed conditions to be attained, which is assured for all test cases used in the present work. Above the measurement location a flow abatement zone with a length of ~10% of the main flow section has been added to ensure that there is no influence of the outlet condition imposed at the top of the domain. A pressure boundary condition is set at the top. On the walls a no-slip condition is used for the liquid phase and a free-slip condition for the gas phase, assuming that direct contacts between the bubbles and the walls are negligible. To avoid the need to resolve the viscous boundary layer, a turbulent wall function is applied, which combines

expressions for the viscous and inertial sublayers. Full details of the presently used implementation in OpenFOAM has already been given in Rzehak and Kriebitzsch (2015). The applied computational grids are uniform in both radial (r-) and axial (z-) directions. Suitable numbers of grid points, N_r and N_z, are taken from previous simulations (Rzehak and Kriebitzsch 2015, Kriebitzsch and Rzehak, 2016) as summarized in Table 3.

Table 2: Summary of computational grids, refer to Table 4 for description of test cases.

test case name	number of radial points N_r	number of axial points N_z
Hosokawa et al. (2009)		
H1x	68	800
H2x	51	800
Liu (1998)		
Lxxx	40	800
MTLoop (Lucas et al. 2005)		
MTxxx	40	800

Detailed descriptions of parameters specific to each case are given in section 4 below. Like in previous works, a fixed monodisperse size distribution with an average bubble size, d_B, taken from the experimental data is assumed. Values of the nominal volumetric fluxes reported in the experimental works often do not agree with the integrals calculated from the measured profiles as

$$J = \frac{8}{D^2} \int_0^{D/2} \alpha(r)\, u(r)\, r\, dr\,. \tag{8}$$

Like in previous works (e.g. Rzehak et al. 2012), the fluxes calculated from the measured profiles, J_{adj}, are used in these cases, since the final comparison is made with these profiles.

Material Properties used correspond to air bubbles in water at atmospheric pressure and 25°C temperature and are summarized in Table 3.

Table 3: Summary of material properties.

liquid density ρ_L	997	kg / m³
liquid viscosity μ_L	8.899e-4	kg / (m s)
gas density ρ_G	1.185	kg / m³
gas viscosity μ_G	1.831e-5	kg / (m s)
surface tension σ	0.072	N / m

4 SIMULATION RESULTS

In line with the purpose of the present work to assess a commonly made approximation in previous simulations of bubbly pipe flow, a selection of test cases considered in those works has been made. Care has been taken to include a certain range of the pertinent parameters such as gas and liquid volumetric fluxes as well as pipe diameter. The data stem from three different experiments with all parameter values summarized in Table 4. The available measurements comprise gas fraction, mean gas and liquid velocities, and liquid turbulent kinetic energy although not all quantities are available in each experiment. However, since the focus of the present work is on comparing simulation models differing in a certain aspect, all quantities are shown throughout. Each of the different experiments is considered in turn.

Table 4: Summary of parameters for the selected tests.

test case name	pipe diameter D mm	pipe length H mm	liquid volume flux $J_{L,adj}$ m/s	gas volume flux $J_{G,adj}$ m/s	mean bubble size $\langle d_B \rangle$ mm	total gas hold-up $\langle \alpha_G \rangle$ %
Hosokawa et al. (2009)						
H11	25.0	2000	0.5	0.018	3.21	2.5
H12			0.5	0.031	4.25	4.1
H21			1.0	0.035	3.52	2.8
H22			1.0	0.042	3.66	3.2
Liu (1998)						
L21B	57.2	3800	1.0	0.14	3.03	10.6
L21C			1.0	0.13	4.22	9.6
L22A			1.0	0.22	3.89	15.7
L11A			0.5	0.12	2.94	15.2
MTLoop (Lucas et al. 2005)						
MT039	51.2	3500	0.4050	0.0111	4.92	1.88
MT050			0.4050	0.0198	4.93	3.25
MT061			0.4050	0.0312	5.22	5.06
MT072			0.4050	0.0496	5.52	7.98
MT041			1.0167	0.0111	4.96	0.96
MT052			1.0167	0.0192	4.95	1.62
MT063			1.0167	0.0309	5.16	2.57
MT074			1.0167	0.0490	5.28	4.03

4.1 Tests from Hosokawa et al. (2009)

Hosokawa and Tomiyama (2009) studied upward vertical flow of water and air in a round pipe with inner diameter D = 25 mm at atmospheric pressure and room temperature. Non-intrusive optical imaging techniques, namely shadowgraphy and LDV were used to measure radial profiles of the gas fraction, mean liquid and gas velocity, and liquid turbulent kinetic energy at an axial location L/D = 68. In addition, an overall distribution of bubble sizes has

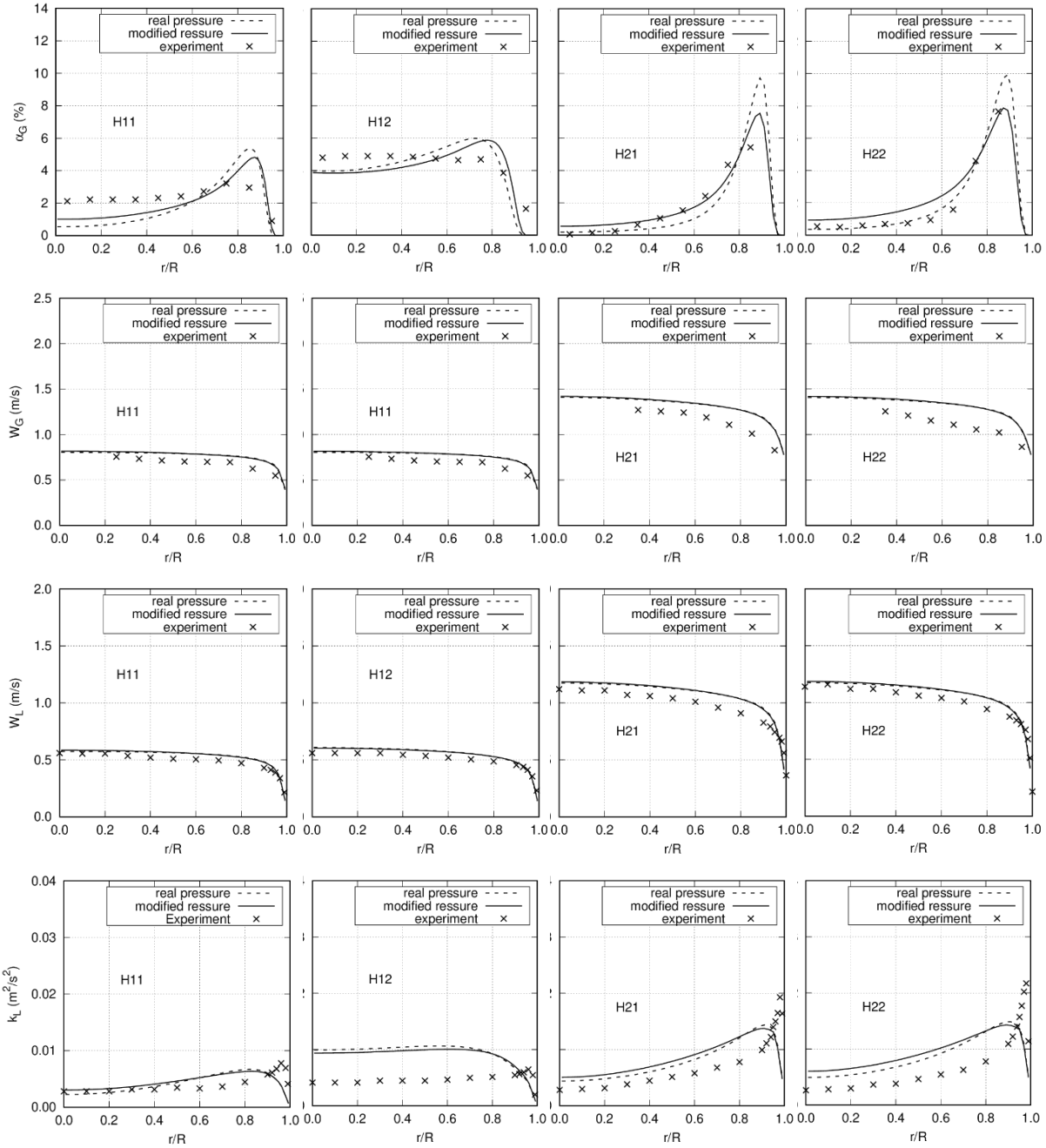

Figure 3: Influence of the pressure term for cases from Hosokawa et al. (2009). Columns show the individual test cases as indicated on each panel, while rows give the different observables, i.e. gas fraction, α_G, vertical component of gas and liquid velocity, u_G and u_L, and liquid turbulent kinetic energy, k_L, from top to bottom. The lines represent simulation results using

the two different models discussed in sections 2 and 3 and symbols represent the experimental available data.

been recorded with equivalent spherical diameters determined from a reconstruction of stereoscopic images. The major characteristics of the test cases are shown in Table 4. There, the average values for the gas fraction are obtained from radial averaging of the profiles while the average values of bubble size are obtained from the measured distributions.

Results for the tests from Hosokawa et al. (2009) are shown in Figure 3 where each column corresponds to one of the test cases and each row gives one observable. For all tests, simulations using the real pressure (dashed lines) rather than the modified one (solid lines) are seen to have an appreciable effect only on the gas fraction, α_G. For the liquid turbulent kinetic energy, k_L, the difference between both pressure treatments is only tiny and for both the gas and liquid mean velocities, u_G and u_L, no influence can be discerned at all. Upon using the real pressure the general trend for the gas fraction profiles is to increase the height of the wall peak somewhat (cases H21 and H22) and to move its location a little bit further away from the wall (cases H11 and H12).

In comparison with the experimental data, the overall agreement is neither improved nor degraded significantly upon using the real pressure formulation. The increased height of the calculated gas fraction peak for cases H21 and H22 tends to differ more from the measurements. However, in these cases, the consequently lowered calculated gas fraction value in the pipe center tends to be closer to the measurements. To more precisely judge the correct behavior in the vicinity of the wall, measurement points at smaller wall distances would be desirable. For cases H11 and H12 the measured profiles are much less peaked than the simulated ones irrespective of the pressure treatment.

4.2 Tests from Liu (1998)

The study of Liu (1998) is concerned with upward vertical flow of water and air in a round pipe with inner diameter D = 57.2 mm. Intrusive techniques, namely a dual needle resistivity probe and a single sensor hot film boundary layer probe were used to measure radial profiles of gas fraction, average bubble size, mean axial liquid velocity, and axial liquid turbulence intensity at an axial position L/D = 60. The average bubble size was computed from measurements of the chord length under the assumption of a spherical bubble shape. The major characteristics of these test cases are again shown in Table 4. The average values for both gas fraction and bubble diameter given there are obtained from radial averaging of the measured profiles. As noted in previous works considering these tests (e.g. Rzehak and Kriebitzsch 2015), when comparing the measured vertical velocity fluctuation w' to the turbulent kinetic energy, k, which is available from the turbulence model, the estimate for isotropic turbulence $k/w' \approx \sqrt{3/2} \approx 1.22$ shows that an overestimate by 20% may be expected.

Simulation results for the tests from Liu (1998) are shown in Figure 4. Qualitatively similar observations as for the tests from Hosokawa et al. (2009) can be made. Quantitatively the difference between using real and modified pressures for the gas fractions is even smaller here and also the deviations from the experimental data are smaller. For the liquid turbulent kinetic energy slightly larger absolute differences between both pressure treatments are seen, but this difference is irrelevant in relation to the deviations from the measurements,

which are rather large here. For the mean gas and liquid velocities, finally, a tiny difference appears between the two simulations and both agree well with the available data except very close to the wall.

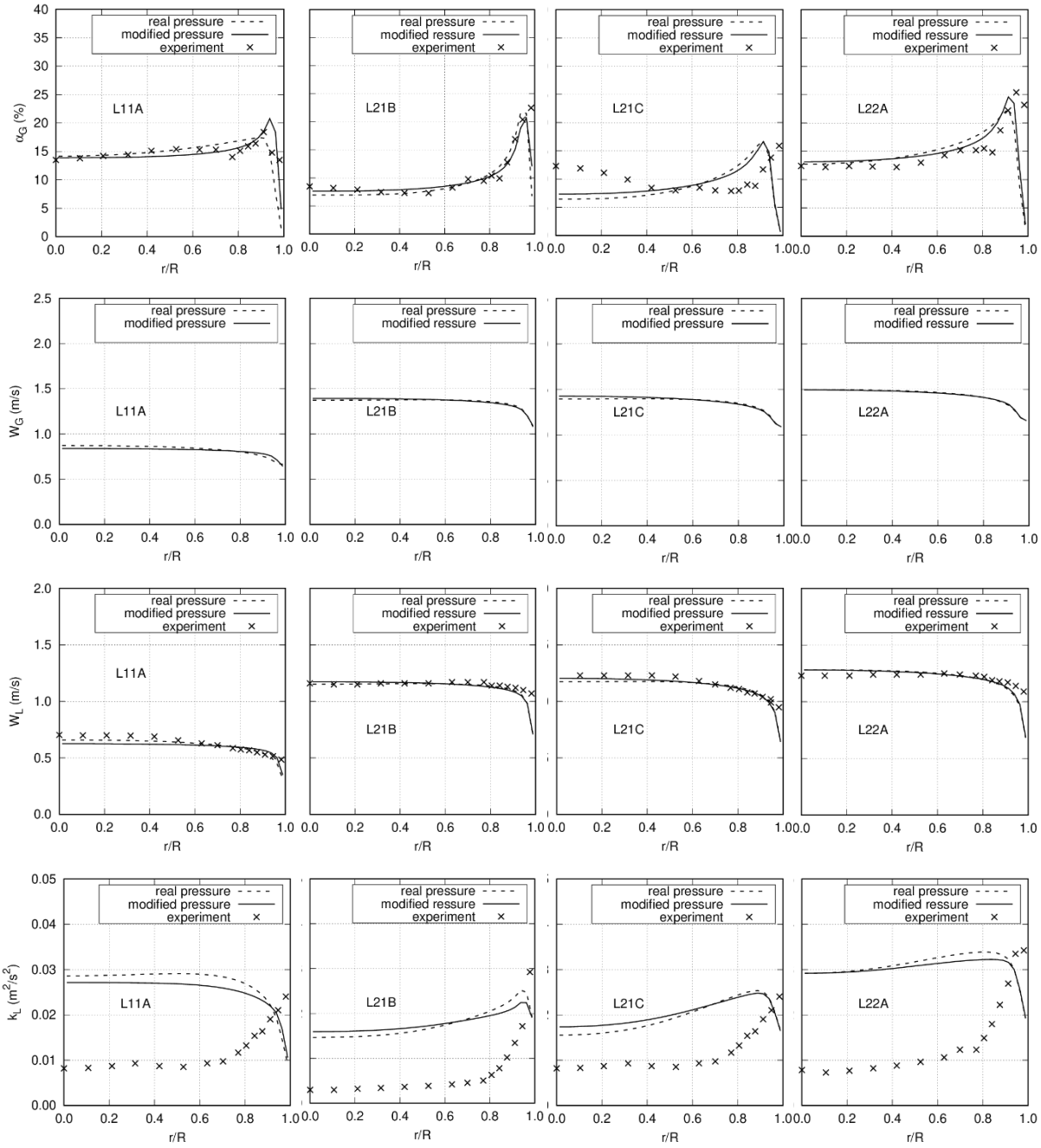

Figure 4: Influence of the pressure term for cases from Liu (1998). Columns show the individual test cases as indicated on each panel, while rows give the different observables, i.e. gas fraction, α_G, vertical component of gas and liquid velocity, u_G and u_L, and liquid turbulent kinetic energy, k_L, from top to bottom. The lines represent simulation results using the two different models discussed in sections 2 and 3 and symbols represent the experimental available data.

4.3 MTLoop Tests (Lucas et al. 2005)

The MTLoop facility was used to study upward vertical flow of air and water, as described in detail in Lucas et al. (2005). The test section consisted of a circular pipe with inner diameter D = 51.2 mm. Measurements at an axial position of L/D = 60 will be considered in the present comparison, where radial profiles of gas volume fraction and gas velocity as well as distributions of bubble size were measured by a wire-mesh sensor. The relevant parameters

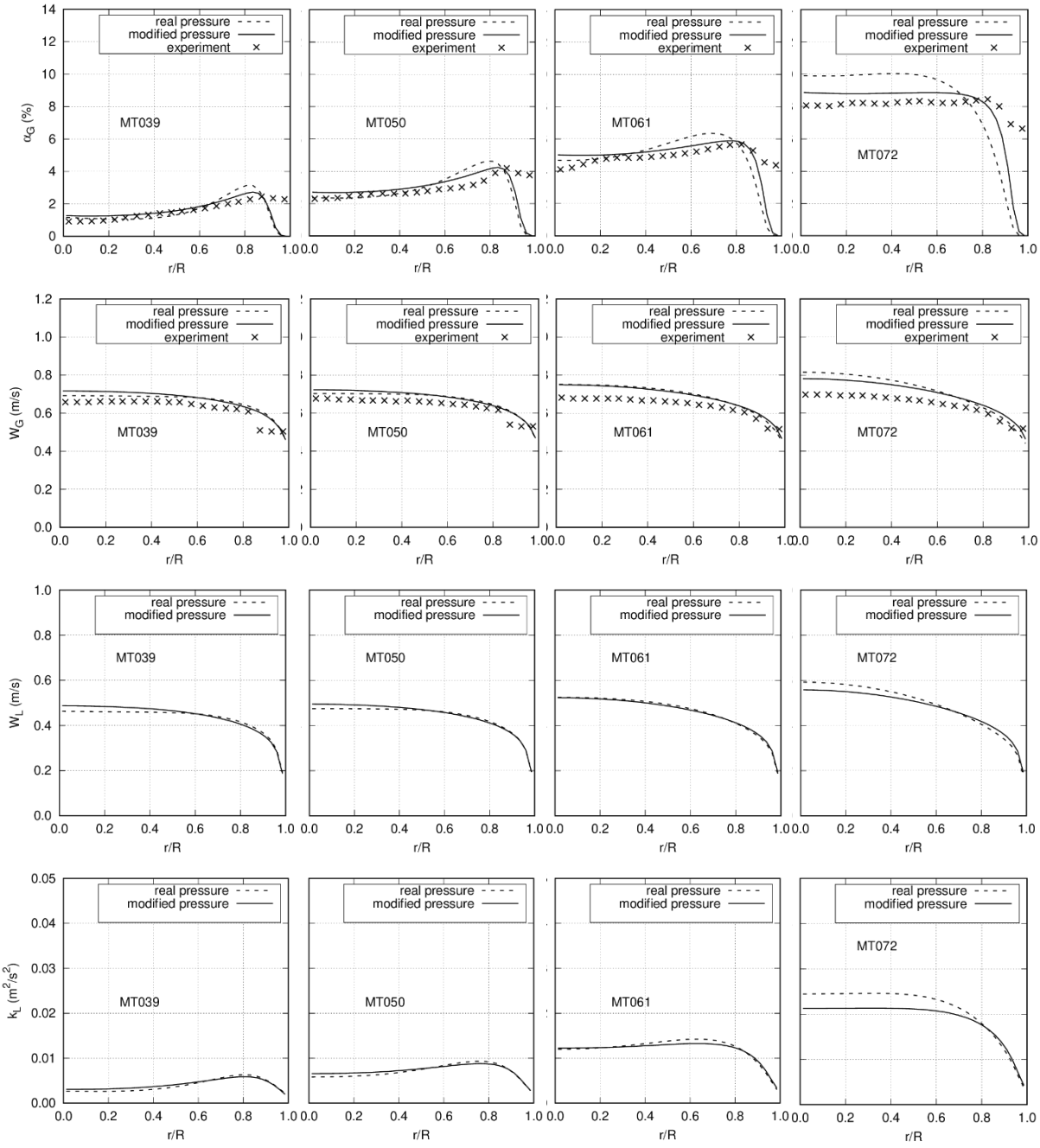

Figure 5: Influence of the pressure term for MTLoop cases (Lucas et al. 2005). Columns show the individual test cases as indicated on each panel, while rows give the different observables, i.e. gas fraction, α_G, vertical component of gas and liquid velocity, u_G and u_L, and liquid turbulent kinetic energy, k_L, from top to bottom. The lines represent simulation results using the two different models discussed in sections 2 and 3 and symbols represent the experimental available data.

are summarized in Table 4 as well. The average values for the gas fraction given there are obtained from radial averaging of the measured profiles, while those for the bubble diameter have been calculated from the measured distributions.

The simulation results for the MTLoop cases shown in Figure 5 and Figure 6 once again exhibit qualitatively similar trends. However, here the difference between usage of the real and modified pressures becomes quite significant for the gas fraction and liquid turbulent kinetic energy at larger values of the gas and liquid volume fluxes, J_G and J_L. A small difference is also seen for the mean velocities of both phases. The trend of having a gas fraction a higher peak somewhat farther away from the wall with correspondingly smaller values in the pipe

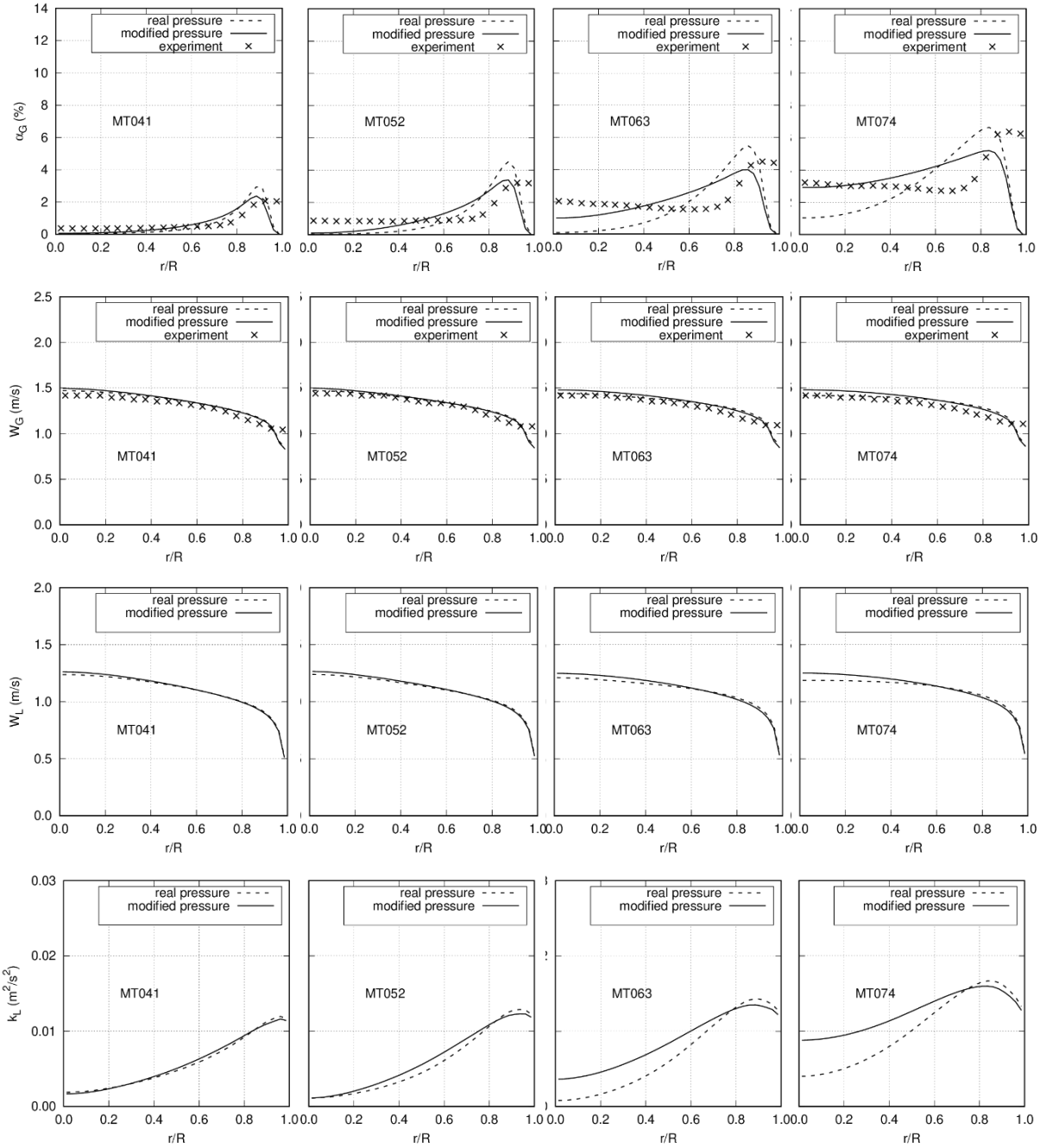

Figure 6: Influence of the pressure term for MTLoop cases (Lucas et al. 2005), continued from Figure 5.

center when the real pressure is used, are seen very clearly in these tests. In addition, the effect on the liquid turbulent kinetic energy is qualitatively the same, which can be explained as a consequence of the bubble-induced contribution to the turbulence, which obviously follows the gas fraction.

Concerning comparison with the measured data it should be noted that the bubble sizes for these tests are somewhat bigger than for the ones of Hosokawa et al. (2009) and Liu (1998) . In particular for the two higher values of the gas volume flux, they come close to the size where a sign reversal of the lift force occurs according to the correlation of Tomiyama et al. which was employed in all simulations (see Table 1). Therefore, as noted in previous works (e.g. Rzehak et al. 2015, Krepper et al. 2019) a treatment with several bubble size groups may be more appropriate for these cases to represent the effects of the inevitably present polydispersity.

5 DISCUSSION AND CONCLUSIONS

Simulations of bubbly pipe flows based on real pressure, i.e. taking into account radial pressure variations due to turbulence, have been compared to corresponding simulations using the so-called modified pressure, in which these variations are neglected. Since pressure gradients exert forces on the bubbles, both treatments lead to different results and the latter has to be considered as an approximation. From a numerical viewpoint, the same setups were found suitable for both models giving similar convergence and runtime.

For the investigated test cases, the effect of using the modified instead of the real pressure is not overly big. The most significant differences are seen in the gas fraction profiles, where typically with the real pressure the wall peak is higher and farther away from the wall than with the modified pressure. A smaller influence with similar trends is found on the turbulent kinetic energy. For the mean gas and liquid velocities the effect is negligible if present at all. In dependence on the flow parameters, the difference between both pressure treatments appears less pronounced at higher total gas content as seen in the tests from Liu (1998). If the total gas content is low, the difference increases with increasing liquid flux, which is prominent in the MTLoop tests (Lucas et al. 2005). Concerning the agreement with the experimental data, there is no distinct overall advantage of one over the other for the investigated set of test cases – either both give reasonable agreement or both are unsatisfactory.

Based on these observations, previous works based on the modified pressure can be largely expected to remain valid. It has to be considered however that the range of flow conditions that were considered is restricted to vertical upward pipe flows and that for certain flow conditions the difference between the pressure treatments is not negligible. Furthermore, the real pressure depends on the turbulent kinetic energy, which is in some cases only poorly predicted in the simulations. In view of these limitations of the present assessment, for future investigations and in particular for more complex flows, use of the real pressure is favored in order to reflect the governing physics as closely as possible. The baseline model proposed in previous works (e.g. Lucas et al. 2016, Rzehak et al. 2017, Liao et al. 2019) will be updated accordingly. Studies extending the present one to cases with other flow conditions and polydisperse bubble size distributions are planned for the future. In particular cases with strongly inhomogeneous turbulence are interesting, since they are more likely to show an

effect of the pressure treatment as the difference between real and modified pressure is proportional to k (see Eq.(4)).

6 ACKNOWLEDGEMENT

This work was partly supported by the Helmholtz European Partnering Programm in the project “Crossing borders and scales (Crossing)”.

7 NOMENCLATURE

Symbol	Unit	Denomination
d_B	m	bubble diameter
D	m	pipe diameter
$\boldsymbol{F}$	N m^{-3}	force per unit volume
g	m s^{-2}	acceleration of gravity
H	m	height of domain
J	m s^{-1}	superficial velocity = volumetric flux
k	m^2 s^{-2}	specific turbulent kinetic energy
L	m	length of test section / measurement level
p	N m^{-2}	pressure
t	s	time
R	m	pipe radius
$\mathbf{S}$	N m^{-2}	deviatoric stress tensor
$\mathbf{T}$	N m^{-2}	stress tensor
$\boldsymbol{u}$	m s^{-1}	mean velocity vector
w	m s^{-1}	vertical component of mean velocity
x	m	axial coordinate
y	m	spanwise coordinate
z	m	vertical coordinate
α	-	phase fraction
ϵ	m^2 s^{-3}	turbulent dissipation rate
μ	kg m^{-1} s^{-1}	dynamic viscosity
ρ	kg m^{-3}	density
σ	N m^{-1}	surface tension
ω	s^{-1}	turbulent frequency

Index	Denomination
eff	effective
G	gas
$inter$	interface
L	liquid
mod	modified
mol	molecular
$turb$	turbulent

vis	viscous
ϕ	any phase

8 REFERENCES

ANSYS, 2018. ANSYS CFX-Solver Theory Guide Release 18. *ANSYS Inc*.

Burns, A. D., Frank, T., Hamill, I., Shi, J.-M., 2004. The Favre averaged drag model for turbulence dispersion in Eulerian multi-phase flows. *Proc. 5th Int. Conf. on Multiphase Flow*, ICMF2004, Yokohama, Japan.

Colombo, M., Fairweather, M. , 2019 Influence of multiphase turbulence modelling on interfacial momentum transfer in two-fluid Eulerian-Eulerian CFD models of bubbly flows. *Chemical Engineering Science* 195, 968–984.

Drew, D. A., Passman, S. L., 1998. Theory of Multicomponent Fluids, *Springer*.

Fleck, S. and Rzehak, R. , 2019. Investigation of bubble plume oscillations by Euler-Euler simulation. *Chemical Engineering Science* 207, 853–861.

Hosokawa, S., Tomiyama, A., Misaki, S. and Hamada, T., 2002. Lateral migration of single bubbles due to the presence of wall. *Proc. ASME Joint U.S.-European Fluids Engineering Division Conference,* FEDSM2002*,* Montreal, Canada.

Hosokawa, S. and Tomiyama, A., 2009. Multi-fluid simulation of turbulent bubbly pipe flow. *Chemical Engineering Science* 64, 5308–5318.

Ishii, M. and Hibiki, T., 2011. Thermo-fluid dynamics of two-phase flow. *Springer*, 2nd ed.

Ishii, M. and Zuber, N., 1979. Drag coefficient and relative velocity in bubbly, droplet or particulate flows. *AIChE Journal* 25, 843–855.

Krauß, M. and Rzehak, R., 2018. Reactive absorption of CO2 in NaOH: An Euler-Euler simulation study. *Chemical Engineering Science* 181, 199–214.

Krepper, E., Rzehak, R., Lucas, D., 2018. Validation of a closure model framework for turbulent bubbly two-phase flow in different flow situations. *Nuclear Engineering and Design* 340, 388–404.

Kriebitzsch, S. and Rzehak, R., 2016. Baseline Model for Bubbly Flows: Simulation of Monodisperse Flow in Pipes of Different Diameters. Fluids 1, 29.

Launder, B., Spalding, D., 1974. The Numerical Computation of Turbulent Flows. *Computer Methods in Applied Mechanics and Engineering* 3, 269–289.

Liao, J., Ziegenhein, T., and Rzehak, R., 2016. Bubbly flow in an airlift column: a CFD study. *Journal of Chemical Technology & Biotechnology* 91, 2904–2915.

Liao, Y., Rzehak, R., Lucas, D., Krepper, E., 2015. Baseline closure model for dispersed bubbly flow: Bubble coalescence and breakup. *Chemical Engineering Science* 122, 336-349.

Liao, Y., Ma, T., Liu, L., Ziegenhein, T., Krepper, E., Lucas, D., 2018. Eulerian modelling of turbulent bubbly flow based on a baseline closure concept. *Nuclear Engineering and Design* 337, 450-459.

Liao, Y., Ma, T., Krepper, E., Lucas, D., Fröhlich, J., 2019. Application of a novel model for bubble-induced turbulence to bubbly flows in containers and vertical pipes. *Chemical Engineering Science* 202, 55-69.

Liu, T. J., 1998. The role of bubble size on liquid phase turbulent structure in two-phase bubbly flow. *3rd International Conference on Multiphase Flow* (ICMF1998), Lyon, France.

Lucas, D., Krepper, E., Prasser, H.-M., 2005. Development of co-current air-water flow in a vertical pipe. *International Journal of Multiphase Flow* 31, 1304–1328.

Lucas, D., Rzehak, R., Krepper, E., Ziegenhein, T., Liao, Y., Kriebitzsch, S., Apanasevich, P., 2016. A strategy for the qualification of multi-fluid approaches for nuclear reactor safety. *Nuclear Engineering and Design* 299, 2–11.

Ma, T., Santarelli, C., Ziegenhein, T., Lucas, D. , Froehlich, J., 2017. Direct numerical simulation–based Reynolds-averaged closure for bubble-induced turbulence. Physical Review Fluids, 2, 034301.

Menter, F. R., 2009. Review of the shear-stress transport turbulence model experience from an industrial perspective. *International Journal of Computational Fluid Dynamics* 23, 305–316.

bin Mohd-Akbar, M., Hayashi, K., Hosokawa, S., and Tomiyama, A., 2012. Bubble tracking simulation of bubble-induced pseudoturbulence. *Multiphase Science and Technology* 24, 197–222.

OpenFOAM Foundation, 2018. OpenFOAM version 6 User Guide, https://openfoam.org.

Parekh, J. and Rzehak, R., 2018. Euler-Euler multiphase CFD-simulation with full Reynolds stress model and anisotropic bubble-induced turbulence. *International Journal of Multiphase Flow* 99, 231–245.

Pope, S. B., 2000. Turbulent Flows, *Cambridge University Press*.

Rzehak, R., Krepper, E., and Lifante, C., 2012. Comparative study of wall-force models for the simulation of bubbly flows. *Nuclear Engineering and Design* 253, 41–49.

Rzehak, R. and Krepper, E., 2013. Bubble-induced turbulence: Comparison of CFD models. *Nuclear Engineering and Design* 258, 57–65.

Rzehak, R. and Krepper, E., 2013a. CFD modeling of bubble-induced turbulence. *International Journal of Multiphase Flow* 55, 138–155.

Rzehak, R. and Krepper, E., 2015. Bubbly flows with fixed polydispersity: Validation of a baseline closure model. *Nuclear Engineering and Design* 287, 108–118.

Rzehak, R. and Kriebitzsch, S., 2015. Multiphase CFD-simulation of bubbly pipe flow: A code comparison. *International Journal of Multiphase Flow* 68, 135–152.

Rzehak, R., Krepper, E., Liao, Y., Ziegenhein, T., Kriebitzsch, S., and Lucas, D., 2015. Baseline model for the simulation of bubbly flows. *Chemical Engineering and Technology* 38, 1972–1978.

Rzehak, R., Krepper, E., 2016. Euler-Euler simulation of mass-transfer in bubbly flows. *Chemical Engineering Science* 155, 459–568.

Rzehak, R., Ziegenhein, T., Kriebitzsch, S., Krepper, E., and Lucas, D., 2017. Unified modeling of bubbly flows in pipes, bubble columns, and airlift columns. *Chemical Engineeing Science* 157, 147–158.

Rzehak, R., Krauß, M., Kovats, P., and Zähringer, K., 2017a. Fluid dynamics in a bubble column: New experiments and simulations. *International Journal of Multiphase Flow* 89, 299–312.

Shi, P. and Rzehak, R., 2017. Bubbly flow in stirred tanks: Euler-Euler / RANS modeling. *Chemical Engineering Science* 190, 419–435.

Tomiyama, A., Tamai, H., Zun, I., and Hosokawa, S., 2002. Transverse migration of single bubbles in simple shear flows. *Chemical Engineering Science* 57, 1849–1858.

Ullrich, M., Krumbein, B., Maduta, R., Jakirlic, S., 2014. An eddy-resolving Reynolds stress model for the turbulent bubbly flow in a square cross-sectioned bubble column. ASME 2014 International Mechanical Engineering Congress and Exposition, IMECE2014, Montreal, Canada.

Wang, S. K., Lee, S. J., Jones, O. C. J., Lahey, R. T. J., 1987. 3-D turbulence structure and phase distribution measurements in bubbly two-phase flows. *International Journal of Multiphase Flow* 13, 327–343.

Wilcox, D. C., 1988. Reassessment of the Scale-Determining Equation for Advanced Turbulence Models. AIAA Journal 26, 1299–1310.

Wilcox, D. C., 2006. Turbulence Modeling for CFD. *DCW-Industries* 3rd ed.

Yeoh, G. H. and Tu, J. Y., 2010. Computational Techniques for Multiphase Flows — Basics and Applications, *Butterworth-Heinemann*.

Ziegenhein, T., Rzehak, R., Krepper, E. and Lucas, D., 2013. Numerical simulation of polydispersed flow in bubble-columns with the inhomogeneous multi-size-group model. *Chemie Ingenieur Technik* 85, 1080–1091.

Ziegenhein, T., Rzehak, R., Ma, T., and Lucas, D., 2017. A unified approach for modeling uniform and non-uniform bubbly flows. *Canadian Journal of Chemical Engineering* 95, 170–179.